ELSEVIER

Comput. Methods Appl. Mech. Engrg. 190 (2001) 4627–4647

Computer methods in applied mechanics and engineering

www.elsevier.com/locate/cma

Consistent tangent matrices for substepping schemes ☆

Agustí Pérez-Foguet, Antonio Rodríguez-Ferran, Antonio Huerta *

Departament de Matemàtica Aplicada III, E.T.S. de Ingenieros de Caminos, Edifici C2, Campus Nord, Universitat Politècnica de Catalunya, E-08034 Barcelona, Spain

Received 17 July 2000; received in revised form 17 July 2000

Abstract

A very simple and general expression of the consistent tangent matrix for substepping time-integration schemes is presented. If needed, the derivatives required for the computation of the consistent tangent moduli can be obtained via numerical differentiation. These two strategies (substepping and numerical differentiation) lead to quadratic convergence in complex nonlinear inelasticity problems. © 2001 Elsevier Science B.V. All rights reserved.

Keywords: Finite element method; Computational plasticity; Quadratic convergence; Substepping; Numerical differentiation; Nonlinear problems

1. Introduction

Consistent tangent matrices [1] are an essential ingredient for the efficient solution via implicit methods of complex problems in nonlinear computational mechanics. The expression of the consistent tangent matrix for a wide variety of material models can be found in the literature. *Consistent* means consistent with the numerical time-integration scheme used to solve the local problems (i.e., the time-integration of the constitutive equation at the Gauss-point level), which is typically the backward Euler or the midpoint rule. Consistent tangent matrices are needed to solve the so-called global problem (i.e., the elastoplastic boundary value problem) with quadratic convergence, via a full Newton–Raphson linearization. The local counterpart is also needed to integrate the local problem and obtain quadratic convergence.

For complex models (for instance, with a highly nonlinear coupling between hardening/softening parameters), the convergence of these local problems can be a major issue, and pose severe restrictions to the time increment. This situation is also found with relatively simple models (i.e., perfect plasticity models) at Gauss points with stress states in zones of high curvature of the yield function. In both cases the plastic corrector often has difficulties in returning back to the yield surface [2].

A possible approach would be to use smaller time-steps. However, this amounts to letting the most restrictive Gauss point control the global problem. Various alternative strategies can be found in the literature. For instance, better initial approximations for the local nonlinear problem can be obtained by defining specific auxiliary predictor surfaces [2], or line-search schemes can be used to enlarge the convergence region of the Newton–Raphson method [3]. These two strategies have been applied successfully to several plasticity models. However, they cannot be regarded as the ultimate solution, especially for problems where complex models are involved.

☆ Partially supported by CICYT, Spain. Grant contract: TAP98-0421.

* Corresponding author.
E-mail address: antonio.huerta@upc.es (A. Huerta).

0045-7825/01/$ - see front matter
PII: S0045-7825(00)00336-4

Another approach, also successfully applied in various situations, is substepping [4,5]. The time-step is subdivided into a number of substeps (which can be different for each Gauss point), and a single-step integration rule is employed within each one. If an explicit rule (forward Euler) is chosen, then no iterations are needed at the local level. In fact, substepping is sometimes used in combination with explicit time-marching schemes for dynamic problems, to meet the stability constrains without resorting to very small time-steps. If an implicit rule (backward Euler or midpoint rule) is preferred, then the corresponding single-step nonlinear problems have to be solved. This can be done, for instance, by means of the standard Newton–Raphson method, eventually combined with any acceleration technique such as auxiliary predictor surfaces or line-search.

If an implicit time-marching scheme is used for the boundary value problem, then global iterations are needed, whatever the choice of the integration rule at the local level (even if an explicit rule is used at the local level, the global problem is implicit). To achieve quadratic convergence with the Newton–Raphson method, the local problem must be consistently linearized.

The major contribution of this paper is the expression of the consistent tangent matrix in the framework of substepping schemes. The proposed expression is general: it can be used for any subdivision of the step into (uniform or nonuniform) substeps, and for any single-step integration scheme within each substep. It is also simple: the expression of the consistent tangent moduli has the same structure of the corresponding scheme without substepping.

From a practical viewpoint, the proposed expression allows to use substepping, thus circumventing the use of very small load increments, and attain quadratic convergence at global level. The substeps at each Gauss point are automatically chosen by monitoring the convergence of the local problem. In many applications, the demand for substepping is concentrated in a reduced number of Gauss points, while substepping is not activated in the rest of the domain. As a consequence, the computational cost of substepping is marginal in comparison with the cost of global equilibrium iterations. These aspects are illustrated by means of some numerical examples regarding the rounded hyperbolic Mohr–Coulomb model [6].

The most involved step in obtaining consistent tangent matrices (either with or without substepping) is computing the derivatives of the constitutive equation with respect to stresses and internal variables. These derivatives are also needed to solve the local problems via the Newton–Raphson method.

For simple models, analytical derivatives are readily available, and this leads to compact, explicit expressions of the consistent tangent matrix. In more complicated models, analytical differentiation is rather more cumbersome. For this reason, a different approach is proposed: derivatives are approximated by means of classical difference schemes. The approximated derivatives are then used to solve the local problems and to compute the consistent tangent matrix. As shown in Refs. [7,8], this approach is both robust and computationally efficient. Quadratic convergence is maintained, provided that adequate difference schemes and step sizes (i.e., the perturbation of the difference scheme) are chosen.

Going beyond Refs. [7,8], where only the single-step backward Euler rule is considered, this paper shows that substepping and numerical differentiation can be combined to obtain the consistent tangent matrix leading to quadratic convergence in complex situations, where (1) analytical derivatives of the constitutive equation are not available and (2) the use of single-step integration rules would demand prohibitively small time-steps. This point is illustrated in some examples with the MRS-Lade model [8–10].

2. Problem statement

2.1. Preliminaries

Many elastoplastic models for small strains can be put in the general form [11]

$$\boldsymbol{\epsilon} = \boldsymbol{\epsilon}^{\mathrm{e}} + \boldsymbol{\epsilon}^{\mathrm{p}}, \quad \boldsymbol{\sigma} = \mathbf{E}\boldsymbol{\epsilon}^{\mathrm{e}}, \quad \dot{\boldsymbol{\epsilon}}^{\mathrm{p}} = \dot{\lambda}\mathbf{m}(\boldsymbol{\sigma}, \boldsymbol{\kappa}), \quad \dot{\boldsymbol{\kappa}} = \dot{\lambda}\mathbf{h}(\boldsymbol{\sigma}, \boldsymbol{\kappa}), \tag{1}$$

where $\boldsymbol{\epsilon}$, $\boldsymbol{\epsilon}^{\mathrm{e}}$ and $\boldsymbol{\epsilon}^{\mathrm{p}}$ are the total, elastic and plastic strain tensors, respectively, $\boldsymbol{\sigma}$ the Cauchy stress tensor, $\mathbf{E}$ the elastic stiffness tensor, $\mathbf{m}$ the flow vector, $\boldsymbol{\kappa}$ the set of internal variables and $\mathbf{h}$ are the plastic moduli. The

plastic multiplier $\dot{\lambda}$ is determined with the aid of the loading–unloading criterion that can be expressed in Kuhn–Tucker form as [12]

$$F(\boldsymbol{\sigma},\boldsymbol{\kappa}) \leqslant 0, \quad \dot{\lambda} \geqslant 0, \quad F(\boldsymbol{\sigma},\boldsymbol{\kappa})\dot{\lambda} = 0, \tag{2}$$

where $F(\boldsymbol{\sigma},\boldsymbol{\kappa})$ is the yield function that defines the admissible stress states.

2.2. Single-step numerical time-integration

Time-integration of Eq. (1) with the backward Euler scheme yields the following nonlinear local problem [11,12]:

$$^{n+1}\boldsymbol{\sigma} + \lambda \mathbf{E}\mathbf{m}\left(^{n+1}\boldsymbol{\sigma}, ^{n+1}\boldsymbol{\kappa}\right) = {}^{n}\boldsymbol{\sigma} + \mathbf{E}\Delta\boldsymbol{\epsilon}, \quad ^{n+1}\boldsymbol{\kappa} - \lambda \mathbf{h}\left(^{n+1}\boldsymbol{\sigma}, ^{n+1}\boldsymbol{\kappa}\right) = {}^{n}\boldsymbol{\kappa}, \quad F\left(^{n+1}\boldsymbol{\sigma}, ^{n+1}\boldsymbol{\kappa}\right) = 0 \tag{3}$$

In Eq. (3), the state at time ^{n}t (i.e., quantities $^{n}\boldsymbol{\sigma}$ and $^{n}\boldsymbol{\kappa}$) and the increment of *total* strains from time ^{n}t to time ^{n+1}t, $\Delta\boldsymbol{\epsilon}$, are known. The unknowns of this local problem are the stresses $^{n+1}\boldsymbol{\sigma}$ and the internal variables $^{n+1}\boldsymbol{\kappa}$ at time ^{n+1}t, and the incremental plastic multiplier λ.

To solve this nonlinear local problem with the Newton–Raphson method, the Jacobian of the residual is needed. Using standard vector notation in computational mechanics [13], the Jacobian at ^{n+1}t can be written as

$$^{n+1}\mathbf{J} = \begin{pmatrix} \left(\mathbf{I}_{n\sigma} + \lambda \mathbf{E}\frac{\partial \mathbf{m}}{\partial \boldsymbol{\sigma}}\right) & \lambda \mathbf{E}\frac{\partial \mathbf{m}}{\partial \boldsymbol{\kappa}} & \mathbf{E}\mathbf{m} \\ -\lambda \frac{\partial \mathbf{h}}{\partial \boldsymbol{\sigma}} & \left(\mathbf{I}_{n\kappa} - \lambda \frac{\partial \mathbf{h}}{\partial \boldsymbol{\kappa}}\right) & -\mathbf{h} \\ \mathbf{n}^{\mathrm{T}} & \boldsymbol{\xi}^{\mathrm{T}} & 0 \end{pmatrix}_{t=^{n+1}t}, \tag{4}$$

where $\mathbf{n}$ and $\boldsymbol{\xi}$ are the derivatives of $F(\boldsymbol{\sigma},\boldsymbol{\kappa})$ with respect to $\boldsymbol{\sigma}$ and $\boldsymbol{\kappa}$, respectively, the superscript T denotes transpose, $n\sigma$ the dimension of the stress vector, $n\kappa$ the number of internal variables and $\mathbf{I}_{*}$ is the identity matrix of order $*$.

In order to solve the local problem, an initial approximation for the unknowns is also needed. The standard choice is the *elastic trial* state, which is

$$^{n+1}\boldsymbol{\sigma}^{0} = {}^{n}\boldsymbol{\sigma} + \mathbf{E}\Delta\boldsymbol{\epsilon}, \quad ^{n+1}\kappa^{0} = {}^{n}\kappa \quad \text{and} \quad \lambda^{0} = 0. \tag{5}$$

Moreover, to solve the global problem with quadratic convergence it is necessary to use the consistent tangent matrix [1,14]. To compute this matrix, the consistent tangent moduli $\mathrm{d}^{n+1}\boldsymbol{\sigma}/\mathrm{d}^{n+1}\boldsymbol{\epsilon}$ at each Gauss point are needed. They are obtained by linearizing Eq. (3). This linearization can be represented in a compact form as [15]

$$\mathbf{P}^{\mathrm{T}}\left(^{n+1}\mathbf{J}\right)^{-1}\mathbf{P}\mathbf{E} \tag{6}$$

where $\mathbf{P}^{\mathrm{T}} = (\mathbf{I}_{n\sigma}, \mathbf{0}_{n\sigma,n\kappa+1})$ is the projection matrix on stress space; note that $\mathbf{0}_{n\sigma,n\kappa+1}$ is a null rectangular matrix with $n\sigma$ rows and $n\kappa + 1$ columns.

2.3. Substepping technique

In some cases, especially with complex material models and when large strain increments are imposed, the local problem with the standard initial approximation, Eq. (5), does not converge. This can be solved using an auxiliary predictor surface in order to find a better initial approximation [2]. However, a specific auxiliary predictor surface must be devised for each material model. A different approach is followed here: an adaptive substepping technique, which is activated when the local problem requires more than a prescribed number of iterations. With this technique, the regions of nonconvergence of the local problem are avoided.

The constitutive law is integrated from ^{n}t to ^{n+1}t in m substeps. This means that it is integrated first from ^{n}t to $^{n+(1/m)}t$, then from $^{n+(1/m)}t$ to $^{n+(2/m)}t$, and up to the last substep, from $^{n+((m-1)/m)}t$ to ^{n+1}t. The integration of the constitutive law is driven by the total strain increment. Thus, the total strain increment from ^{n}t to

${}^{n+1}t$, $\Delta\boldsymbol{\epsilon}$, is divided in m parts (not necessarily equal), one for each substep. The following division is considered:

$$\Delta\boldsymbol{\epsilon} = \Delta\boldsymbol{\epsilon}_1 + \Delta\boldsymbol{\epsilon}_2 + \cdots + \Delta\boldsymbol{\epsilon}_m = \sum_{k=1}^{m} \Delta\boldsymbol{\epsilon}_k = \sum_{k=1}^{m} \alpha_k \Delta\boldsymbol{\epsilon}. \tag{7}$$

Each substep is integrated with a single-step scheme. Except in trivial cases, each substep is a nonlinear problem. Obviously, these problems have the same structure of the local problem if the constitutive law is integrated directly from ${}^{n}t$ to ${}^{n+1}t$ with the same single-step scheme. Here the backward Euler scheme is used. Nevertheless, Appendix A shows the consistent tangent moduli for substepping with the generalized midpoint rule.

The nonlinear problem corresponding to a generic substep k integrated with the backward Euler method can be expressed as

$$\mathbf{f}\left({}^{n+(k/m)}\boldsymbol{\sigma}, {}^{n+(k/m)}\boldsymbol{\kappa}, \lambda_k\right) = \begin{pmatrix} \mathbf{I}_{n\sigma} & \mathbf{0}_{n\sigma,n\kappa} & \mathbf{0}_{n\sigma,1} \\ \mathbf{0}_{n\kappa,n\sigma} & \mathbf{I}_{n\kappa} & \mathbf{0}_{n\kappa,1} \\ \mathbf{0}_{1,n\sigma} & \mathbf{0}_{1,n\kappa} & 0 \end{pmatrix} \begin{pmatrix} {}^{n+(k-1/m)}\boldsymbol{\sigma} \\ {}^{n+(k-1/m)}\boldsymbol{\kappa} \\ \lambda_{k-1} \end{pmatrix} + \begin{pmatrix} \mathbf{E} \\ \mathbf{0}_{n\kappa,1} \\ 0 \end{pmatrix} \Delta\boldsymbol{\epsilon}_k \tag{8}$$

with $\mathbf{f}$ defined as

$$\mathbf{f}\left({}^{n+(k/m)}\boldsymbol{\sigma}, {}^{n+(k/m)}\boldsymbol{\kappa}, \lambda_k\right) = \begin{pmatrix} {}^{n+(k/m)}\boldsymbol{\sigma} + \lambda_k \mathbf{Em}\left({}^{n+(k/m)}\boldsymbol{\sigma}, {}^{n+(k/m)}\boldsymbol{\kappa}\right) \\ {}^{n+(k/m)}\boldsymbol{\kappa} - \lambda_k \mathbf{h}\left({}^{n+(k/m)}\boldsymbol{\sigma}, {}^{n+(k/m)}\boldsymbol{\kappa}\right) \\ F\left({}^{n+(k/m)}\boldsymbol{\sigma}, {}^{n+(k/m)}\boldsymbol{\kappa}\right) \end{pmatrix}. \tag{9}$$

Eqs. (8) and (9) represent the extension of Eq. (3) to the case of substepping. They are valid for any substep ($k \in \{1, \ldots, m\}$) within the time-step. For a given instant ${}^{n+(i/m)}t$, the stresses and the internal variables are ${}^{n+(i/m)}\boldsymbol{\sigma}$ and ${}^{n+(i/m)}\boldsymbol{\kappa}$, respectively, whereas the incremental plastic multiplier of the substep i (from time ${}^{n+((i-1)/m)}t$ to ${}^{n+(i/m)}t$) is λ_i. In Eq. (8) everything is known at $i = k-1$, and must be computed for $i = k$, except for $\Delta\boldsymbol{\epsilon}_k$ which is the prescribed total strain increment of substep k.

Note that, in fact, λ_{k-1} is not involved in Eq. (8). It has been included in order to simplify the development of the consistent tangent matrix in Section 3.

3. The consistent tangent matrix for the substepping technique

To compute the consistent tangent matrix for the substepping technique, the corresponding consistent tangent moduli $\mathrm{d}^{n+1}\boldsymbol{\sigma}/\mathrm{d}^{n+1}\boldsymbol{\epsilon}$ at each Gauss point are needed. They are obtained by linearizing recursively the m systems of equations solved to integrate the constitutive equation with substepping, i.e., Eq. (8) for $k = 1, \ldots, m$. In order to linearize these m systems of equations, it is necessary to highlight the dependence of ${}^{n+1}\boldsymbol{\sigma}$ on $\Delta\boldsymbol{\epsilon}$.

The stresses ${}^{n+1}\boldsymbol{\sigma}$ are defined implicitly, together with ${}^{n+1}\boldsymbol{\kappa}$, as functions of ${}^{n+((m-1)/m)}\boldsymbol{\sigma}$, ${}^{n+((m-1)/m)}\boldsymbol{\kappa}$ and $\Delta\boldsymbol{\epsilon}_m$. The dependence of $\Delta\boldsymbol{\epsilon}_m$ on $\Delta\boldsymbol{\epsilon}$ is simple, $\Delta\boldsymbol{\epsilon}_m = \alpha_m \Delta\boldsymbol{\epsilon}$. But the stresses ${}^{n+((m-1)/m)}\boldsymbol{\sigma}$ and the internal variables ${}^{n+((m-1)/m)}\boldsymbol{\kappa}$ are defined as functions of ${}^{n+((m-2)/m)}\boldsymbol{\sigma}$, ${}^{n+((m-2)/m)}\boldsymbol{\kappa}$ and $\Delta\boldsymbol{\epsilon}_{m-1}$. In fact, the dependence of stresses and internal variables at ${}^{n+(k/m)}t$, with $k = m, \ldots, 1$, on the state at ${}^{n+((k-1)/m)}t$ and $\Delta\boldsymbol{\epsilon}_k$ always has the same structure. The process finishes at $k = 1$, because ${}^{n+(1/m)}\boldsymbol{\sigma}$ and ${}^{n+(1/m)}\boldsymbol{\kappa}$ depend only on $\Delta\boldsymbol{\epsilon}_1 = \alpha_1 \Delta\boldsymbol{\epsilon}$. Note that ${}^{n}\boldsymbol{\sigma}$ and ${}^{n}\boldsymbol{\kappa}$ are inputs of the integration from ${}^{n}t$ to ${}^{n+1}t$.

3.1. The consistent tangent moduli

The m systems of equations are linearized: first a generic substep k, with $k = m, \ldots, 2$, is shown, then the first substep ($k = 1$) is presented. A different treatment is required for the first substep because it depends only on $\Delta\boldsymbol{\epsilon}_1$. Finally, the expression of the consistent tangent moduli is presented.

Both sides of Eq. (8) are linearized with respect to $\Delta\boldsymbol{\epsilon}$,

$$\frac{\mathrm{d}\mathbf{f}}{\mathrm{d}\left({}^{n+(k/m)}\boldsymbol{\sigma},\,{}^{n+(k/m)}\boldsymbol{\kappa},\,\lambda_k\right)}\frac{\mathrm{d}\left({}^{n+(k/m)}\boldsymbol{\sigma},\,{}^{n+(k/m)}\boldsymbol{\kappa},\,\lambda_k\right)}{\mathrm{d}\Delta\boldsymbol{\epsilon}} = \begin{pmatrix}\mathbf{I}_{n\sigma+n\kappa} & \mathbf{0}_{n\sigma,n\kappa,1}\\ \mathbf{0}_{1,n\kappa,n\sigma} & 0\end{pmatrix}\frac{\mathrm{d}\left({}^{n+((k-1)/m)}\boldsymbol{\sigma},\,{}^{n+((k-1)/m)}\boldsymbol{\kappa},\,\lambda_{k-1}\right)}{\mathrm{d}\Delta\boldsymbol{\epsilon}} + \begin{pmatrix}\mathbf{E}\\ \mathbf{0}_{n\kappa,n\sigma}\\ \mathbf{0}_{1,n\sigma}\end{pmatrix}\frac{\mathrm{d}\Delta\boldsymbol{\epsilon}_k}{\mathrm{d}\Delta\boldsymbol{\epsilon}}, \tag{10}$$

where

$$\frac{\mathrm{d}\mathbf{f}}{\mathrm{d}\left({}^{n+(k/m)}\boldsymbol{\sigma},\,{}^{n+(k/m)}\boldsymbol{\kappa},\,\lambda_k\right)} = {}^{n+(k/m)}\mathbf{J} = \begin{pmatrix}\left(\mathbf{I}_{n\sigma}+\lambda\mathbf{E}\frac{\partial\mathbf{m}}{\partial\boldsymbol{\sigma}}\right) & \lambda\mathbf{E}\frac{\partial\mathbf{m}}{\partial\boldsymbol{\kappa}} & \mathbf{E}\mathbf{m}\\ -\lambda\frac{\partial\mathbf{h}}{\partial\boldsymbol{\sigma}} & \left(\mathbf{I}_{n\kappa}-\lambda\frac{\partial\mathbf{h}}{\partial\boldsymbol{\kappa}}\right) & -\mathbf{h}\\ \mathbf{n}^{\mathrm{T}} & \boldsymbol{\xi}^{\mathrm{T}} & 0\end{pmatrix}_{t={}^{n+(k/m)}t} \tag{11}$$

and

$$\frac{\mathrm{d}\Delta\boldsymbol{\epsilon}_k}{\mathrm{d}\Delta\boldsymbol{\epsilon}} = \alpha_k\mathbf{I}_{n\sigma}. \tag{12}$$

Note that the first matrix in the RHS of Eq. (10) is simply a compact expression of a matrix already encountered in Eq. (8).

Assuming that $\det({}^{n+(k/m)}\mathbf{J}) \neq 0$, Eq. (10) is transformed into

$$\frac{\mathrm{d}\left({}^{n+(k/m)}\boldsymbol{\sigma},\,{}^{n+(k/m)}\boldsymbol{\kappa},\,\lambda_k\right)}{\mathrm{d}\Delta\boldsymbol{\epsilon}} = \left({}^{n+(k/m)}\mathbf{J}\right)^{-1}\begin{pmatrix}\mathbf{I}_{n\sigma+n\kappa} & \mathbf{0}_{n\sigma+n\kappa,1}\\ \mathbf{0}_{1,n\sigma+n\kappa} & 0\end{pmatrix} \times\left(\frac{\mathrm{d}\left({}^{n+((k-1)/m)}\boldsymbol{\sigma},\,{}^{n+((k-1)/m)}\boldsymbol{\kappa},\,\lambda_{k-1}\right)}{\mathrm{d}\Delta\boldsymbol{\epsilon}} + \alpha_k\begin{pmatrix}\mathbf{E}\\ \mathbf{0}_{n\kappa,n\sigma}\\ \mathbf{0}_{1,n\sigma}\end{pmatrix}\right), \tag{13}$$

which can be rewritten as

$$\frac{\mathrm{d}\left({}^{n+(k/m)}\boldsymbol{\sigma},\,{}^{n+(k/m)}\boldsymbol{\kappa},\,\lambda_k\right)}{\mathrm{d}\Delta\boldsymbol{\epsilon}} = {}^{n+(k/m)}\mathbf{A}\left(\alpha_k\mathbf{P}\mathbf{E} + \frac{\mathrm{d}\left({}^{n+((k-1)/m)}\boldsymbol{\sigma},\,{}^{n+((k-1)/m)}\boldsymbol{\kappa},\,\lambda_{k-1}\right)}{\mathrm{d}\Delta\boldsymbol{\epsilon}}\right) \tag{14}$$

using $\mathbf{P}^{\mathrm{T}} = (\mathbf{I}_{n\sigma}, \mathbf{0}_{n\sigma,n\kappa+1})$ and

$${}^{n+(k/m)}\mathbf{A} = \left({}^{n+(k/m)}\mathbf{J}\right)^{-1}\begin{pmatrix}\mathbf{I}_{n\sigma+n\kappa} & \mathbf{0}_{n\sigma+n\kappa,1}\\ \mathbf{0}_{1,n\sigma+n\kappa} & 0\end{pmatrix}. \tag{15}$$

Eq. (14) is valid for $k = m, \ldots, 2$. For $k = 1$, the first substep, Eq. (8) is linearized as follows:

$$\frac{\mathrm{d}\left({}^{n+(1/m)}\boldsymbol{\sigma},\,{}^{n+(1/m)}\boldsymbol{\kappa},\,\lambda_1\right)}{\mathrm{d}\Delta\boldsymbol{\epsilon}} = \alpha_1\left({}^{n+(1/m)}\mathbf{J}\right)^{-1}\begin{pmatrix}\mathbf{E}\\ \mathbf{0}_{n\kappa,n\sigma}\\ \mathbf{0}_{1,n\sigma}\end{pmatrix} = \alpha_1\,{}^{n+(1/m)}\mathbf{A}\mathbf{P}\mathbf{E}. \tag{16}$$

The final expression is obtained after substitution of Eq. (16) into Eq. (14) particularized at $k = 2$, and a recursive use of (14) from $k = 3$ up to $k = m$. Finally,

$$\frac{\mathrm{d}\left({}^{n+1}\boldsymbol{\sigma},\,{}^{n+1}\boldsymbol{\kappa},\,\lambda_m\right)}{\mathrm{d}\Delta\boldsymbol{\epsilon}} = {}^{n+1}\mathbf{A}\Big(\alpha_m\mathbf{P}\mathbf{E} + {}^{n+((m-1)/m)}\mathbf{A}\Big(\alpha_{m-1}\mathbf{P}\mathbf{E} + \cdots\big(\alpha_2\mathbf{P}\mathbf{E} + \alpha_1\,{}^{n+(1/m)}\mathbf{A}\mathbf{P}\mathbf{E}\underbrace{\big)\cdots\big)\Big)}_{m-1}. \tag{17}$$

The consistent tangent moduli are in the leading principal minor of order $n\sigma$ of the LHS of Eq. (17). They are obtained by means of the projection matrix $\mathbf{P}$, and have the compact expression

$$\frac{\mathrm{d}^{n+1}\boldsymbol{\sigma}}{\mathrm{d}\Delta\boldsymbol{\epsilon}} = \mathbf{P}^{\mathrm{T}}\left[\sum_{i=1}^{m}\left(\alpha_i \prod_{j=m}^{i} {}^{n+(j/m)}\mathbf{A}\right)\right]\mathbf{P}\mathbf{E}. \tag{18}$$

Eq. (18) has the same structure of Eq. (6). The summation in brackets of Eq. (18) plays the same role that the inverse of the Jacobian of Eq. (6). In fact, Eq. (18) is identical to Eq. (6) if only one substep is considered, $m = 1$.

Note that the computation of the consistent tangent moduli involves matrix inversions, even in the case of single-step integration rules with no substepping, Eq. (6). It must be remarked, however, that small matrices are considered, so numerical inversion poses no difficulties. The order of the Jacobian matrices to be inverted is only $n\sigma + n\kappa + 1$, see Eqs. (4) and (11), and it can be further reduced. A computationally efficient expression of the consistent tangent moduli, with smaller matrices and a recursive structure, is presented in Appendix B.

4. Examples

In this section, two global problems are solved using the consistent tangent matrix for substepping presented in Section 3. Quadratic convergence is attained.

The first example is the simulation of a rigid footing with the rounded hyperbolic Mohr–Coulomb model. When solving this problem with single-step integration rules, the Gauss points located under the corner of the footing restrict the load increment to a forbidding small value. When substepping is used, on the contrary, the load increment no longer depends on local demands. As a consequence, larger load increments can be used. Until now, the use of substepping was incompatible with quadratic convergence at the global level. However, thanks to the consistent tangent matrix presented in Section 3, quadratic convergence results are presented in Section 4.1.

The second example is the simulation of a triaxial test with the MRS-Lade model. In this example, substepping is combined with numerical differentiation. For the MRS-Lade model, not all the derivatives needed to compute the Jacobian of the residual, Eq. (4), have a readily available analytical expression. Because of this, and following Refs. [7,8], numerical differentiation is used to approximate the Jacobian. In these references, numerical differentiation is combined with the backward Euler integration rule and quadratic convergence is obtained at local and global level. In Section 4.2, numerical differentiation is combined with substepping and quadratic results are also obtained.

4.1. Simulation of a rigid footing with the rounded hyperbolic Mohr–Coulomb model

In this section, a rigid footing is analysed with the rounded hyperbolic Mohr–Coulomb model [6] and substepping. The consistent tangent matrix developed in Section 3 is employed to achieve quadratic convergence at the global level.

The model is presented in Ref. [6]. The flow potential–yield surface is divided into two regions: one corresponding to the hyperbolic Mohr–Coulomb zone that smoothes the apex of the classical Mohr–Coulomb model on the hydrostatic axis, and the other corresponding to the rounding zones, that smoothes the corners present on the deviatoric plane. The traces of the flow potential–yield surface on the meridian and the deviatoric planes are presented in Fig. 1. The dimensionless material parameters are a cohesion of 1, a friction angle of 30°, a Young modulus of 3000 and a Poisson coefficient of 0.3. Associated plasticity is considered.

First, the convergence of the local problem is analysed. Fig. 2 depicts the number of iterations for convergence (up to a tolerance of 10^{-12}) with the standard initial approximation, Eq. (5). Note that the Newton–Raphson method does not converge in 10 iterations in some regions of the stress space. This is due to the high curvature of the yield function close to the apex ($I_1/3 \geqslant 0$) combined with the nondifferentiability of the flow vector at $|\theta| = 25°$. In order to avoid these regions of nonconvergence of the local

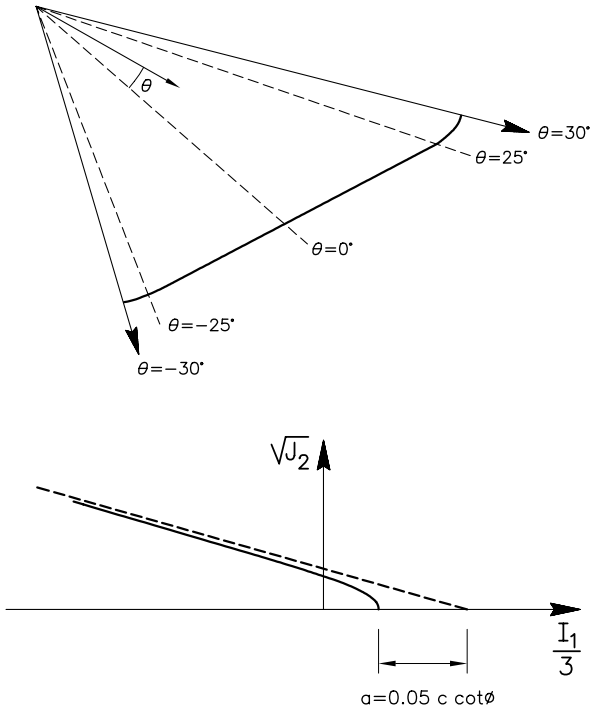

Fig. 1. Main features of the rounded hyperbolic Mohr–Coulomb yield surface: trace on the deviatoric and meridian plane.

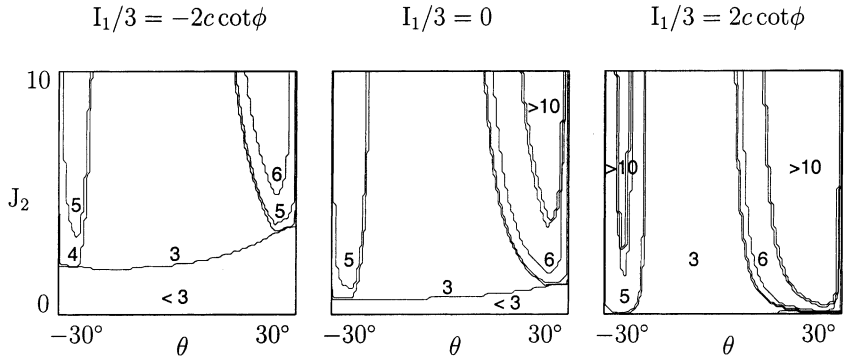

Fig. 2. Rounded hyperbolic Mohr–Coulomb model. Number of iterations of the local problem for trial stresses in the deviatoric plane (θ–J_2) at various levels of confinement ($I_1/3$).

problem, the adaptive substepping scheme is activated at the Gauss points that require more than six iterations at the local level for convergence (to a tolerance of 10^{-12}).

Due to symmetry, only one-half of domain is considered for the global problem, see Fig. 3. The soil mass is modelled as a square of 20 units of length (u.l.), 20 times the footing half-width. It has been checked that this domain is large enough to preclude any undesired influence of the boundary on the results. An unstructured mesh of 1784 quadrilateral eight-noded elements is used. A vertical displacement of the footing of 0.1 u.l. is prescribed in 100, 200, 400 and 800 uniform increments.

The relationship between force and vertical displacement is depicted in Fig. 4. The computed limit dimensionless force is 30.71, 2% above the exact Prandtl collapse dimensionless force of 30.14. Fig. 5 shows the distribution of equivalent plastic strain for different values of the load level (i.e., fraction of the total prescribed displacement). Note that the failure mechanism is well captured. Very similar results are obtained for the four problems, with 100, 200, 400 and 800 load increments (l.i.).

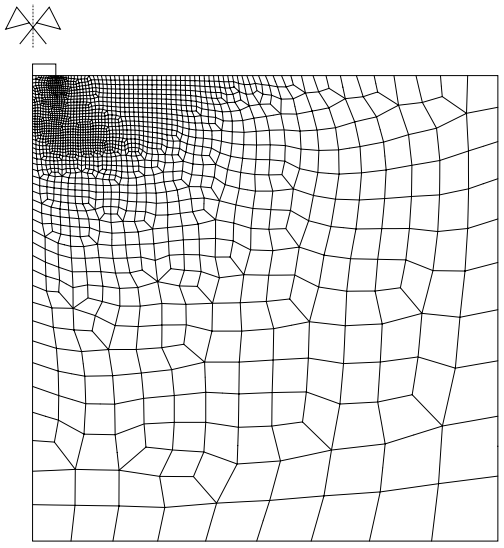

Fig. 3. Rigid footing problem. Computational domain and mesh.

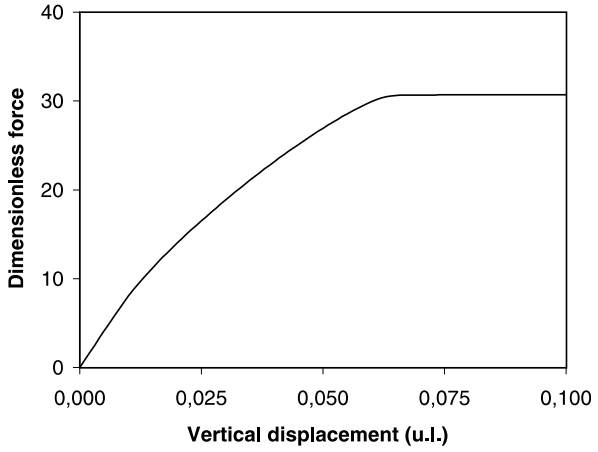

Fig. 4. Rigid footing problem. Dimensionless force versus vertical displacement.

The substepping has been activated just under the right corner of the footing. This agrees with the fact that the nonconvergence regions of the local problem are close to the rounded apex. Fig. 6 shows the evolution of the number of Gauss points with substepping activated, the sum of substeps over all the domain and the maximum number of substeps for all the Gauss points, for the problem solved with 100, 200, 400 and 800 l.i. The number of Gauss points with substepping activated is not very different in the four problems (it is reduced by a factor of less than 2 when the number of load increments increases by a factor of 8). On the other hand, the total number of substeps and the maximum number of substeps are in inverse proportion to the number of steps; if the number of load increments is doubled, then the maximum number of substeps is divided by two. This indicates that a very large number of steps would be needed to solve the problem without substepping (extrapolating the results of Fig. 6, the number of uniform l.i. would be greater than 50 000).

The convergence results for several load levels and for the four problems (with 100, 200, 400 and 800 l.i.) are shown in Fig. 7. All the results are quadratic. As expected, the number of iterations per load increment decreases as the number of load increments increases. In fact, the problem with 100 l.i.

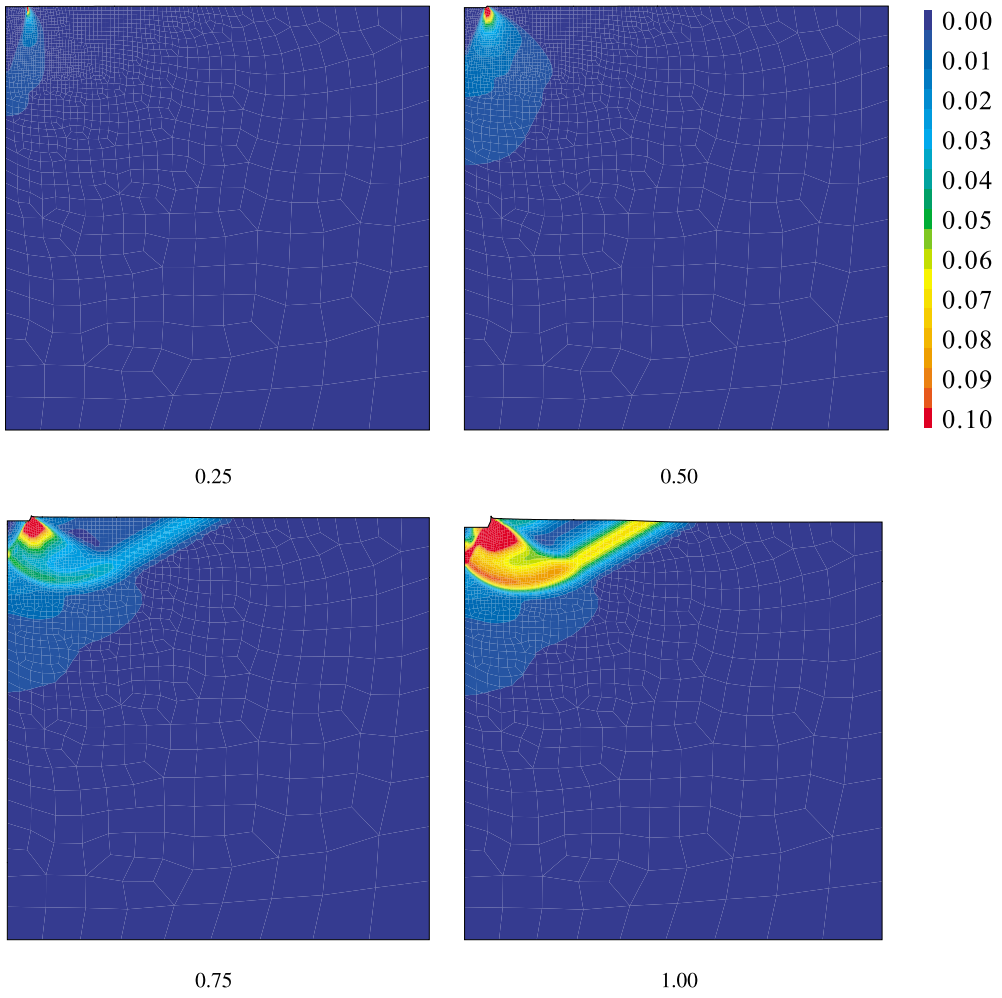

Fig. 5. Rigid footing problem. Equivalent plastic strain for different load levels.

requires up to 11 Newton–Raphson iterations at the increments previous to the plateau in the load–displacement curve. This indicates that larger increments should not be used in this part of the problem.

It has been checked that the influence of the substepping criterion is marginal. If the threshold for activating the substepping is set at 12 iterations (instead of 6), then the same results are found (except for the sum of substeps over the domain, which is a little lower).

The computational cost of the four load discretizations is compared in Table 1 (relative CPU time) and in Fig. 8 (accumulated iterations). The computational cost increases with the number of load increments. Within the range presented in Table 1, twice the number of load increments implies a computational cost 1.6 times greater. The case with no substepping (i.e., 50 000 uniform increments) is also shown in Fig. 8. Note that the computational cost is much higher: the number of accumulated iterations exceeds 10 000 after

Table 1
Rigid footing problem. Relationship between number of global load increments and relative CPU time

Load increments	100	200	400	800
Relative CPU time	100%	160%	263%	432%

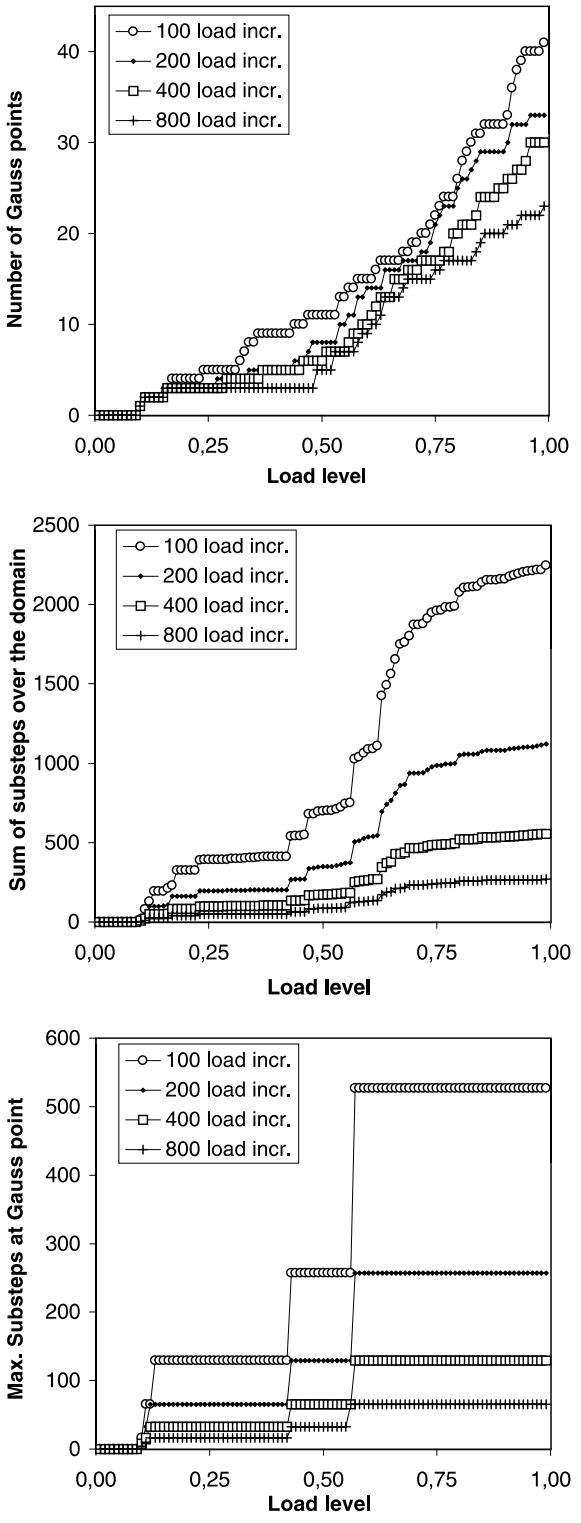

Fig. 6. Rigid footing problem. Evolution of the number of Gauss points with substepping activated (top), the sum of substeps over the domain (center) and the maximum number of substeps for all the Gauss points (bottom).

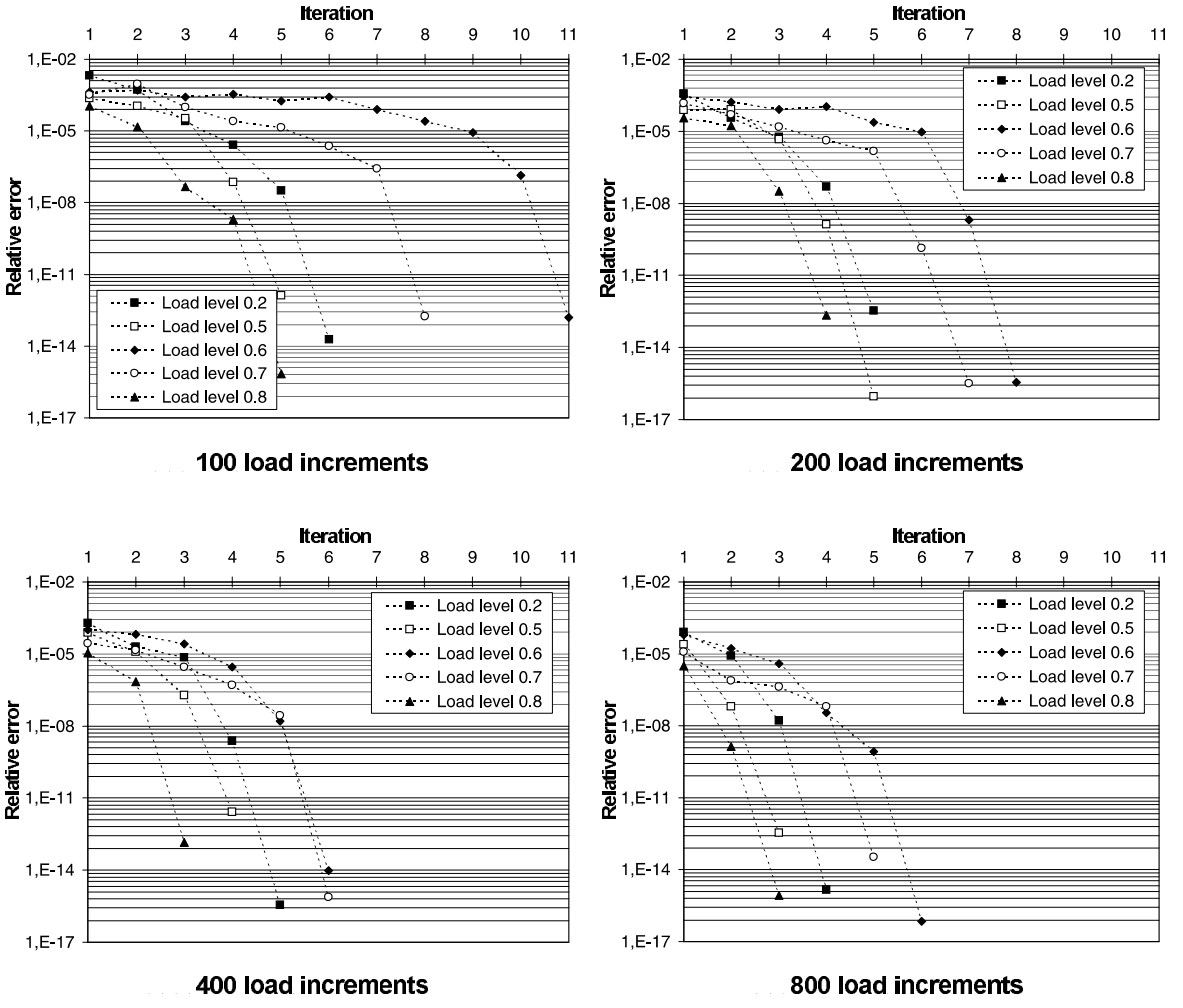

Fig. 7. Rigid footing problem. Convergence results for different load levels.

only one-eighth of the analysis. This clearly illustrates the computational efficiency of the substepping scheme with consistent tangent matrix.

4.2. Triaxial test with the MRS-Lade model

In this section, a triaxial test with end-platen friction is analysed with the MRS-Lade model [8–10] and substepping. The MRS-Lade model is used to simulate the behaviour of granular materials under both low and high confinement stresses [16,17]. It features (1) a two-surface yield function, comprising a smooth cone surface and a smooth cap surface, (2) hardening and softening variables that depend on dissipated plastic work, and (3) a nonassociated flow rule in the meridian plane of the cone region. Several slight modifications to the original formulation of the model have been devised [10,17,18]. In this paper, the modification presented in Ref. [10] is used. It consists of a new definition of the flow vector for the cone region that avoids the corner problem or the flip-over of previous formulations.

The traces of the yield surface on the meridian plane and on the deviatoric plane are depicted in Fig. 9, and the hardening/softening function $\eta_{\mathrm{con}}(\kappa_{\mathrm{con}})$ of the cone in Fig. 10. The value of η_{con} is directly related to the friction angle (slope of the cone in the meridian plane) and κ_{con} is the cone internal variable, which depends on the plastic work. The softening at Gauss point level starts for $\kappa_{\mathrm{con}} = 1$.

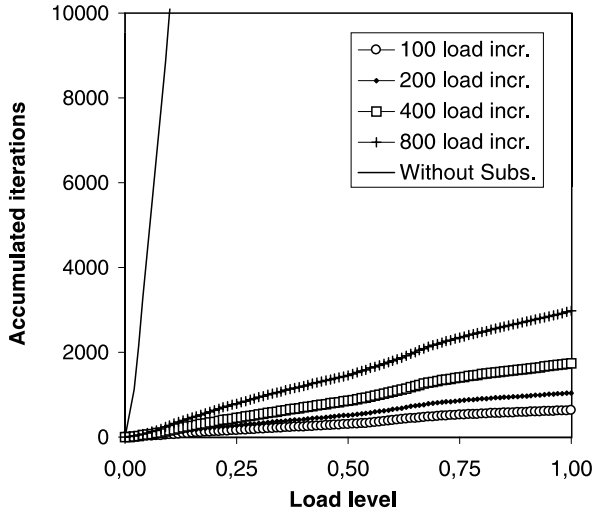

Fig. 8. Rigid footing problem. Relationship between accumulated iterations and load level.

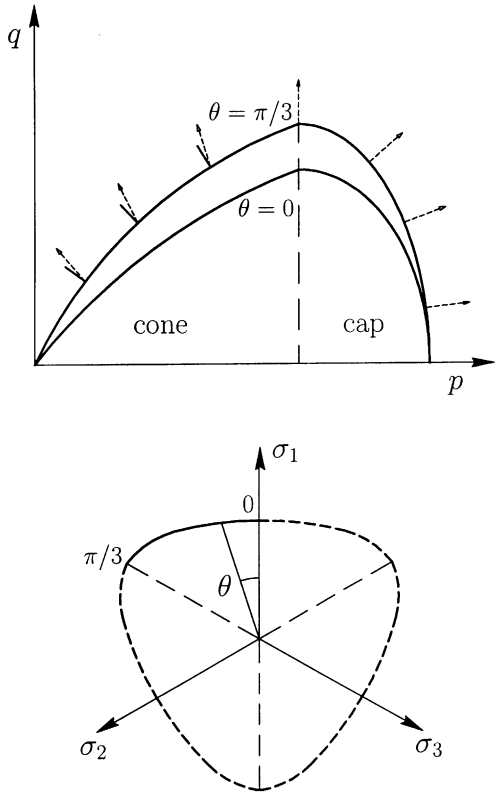

Fig. 9. MRS-Lade model. Traces of the yield criterion on the meridian and on the deviatoric plane.

The MRS-Lade model exhibits a high coupling between the flow vector and the plastic moduli. This coupling makes the analytical computation of the derivatives a very cumbersome task. However, using any of the numerical differentiation techniques presented in Ref. [8], all the derivatives are computed in a simple and efficient way.

Going beyond Refs. [7,8], substepping and numerical differentiation are combined here. Like in the first example, the adaptive substepping technique is activated at the Gauss points where the local problem

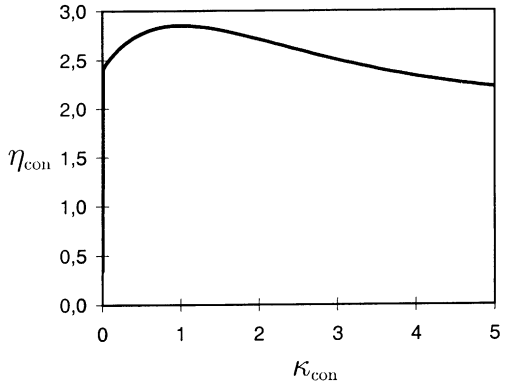

Fig. 10. MRS-Lade model. Hardening/softening function of the cone.

requires more than six iterations for convergence (up to a tolerance of 10^{-12}). As shown in Ref. [8], quadratic convergence at the local level is obtained in all the stress-internal variable space, even with large total strain increments and no substepping. Substepping is used for this problem to ensure proper time-integration of the constitutive law and a reduction of the computational cost, not to avoid nonconvergence regions as in Section 4.1.

A structured mesh of 1350 (30×45) quadrilateral eight-noded elements has been used. Due to double symmetry only the upper right quarter of the sample is modelled. The end-platen friction is imposed by restraining the radial displacement of the sample top during loading. The same material parameters used by Macari et al. [17] to simulate the triaxial test at local level of a Sacramento River sand are used in this example. Since the MRS-Lade model is not regularized and includes nonassociated plasticity and softening, the problem can localize. However, the low degree of softening of the material parameters used and the axisymmetric nature of the test prevent localization [19]. The results do not depend significantly on the space or time discretization. The problem has been solved with 10, 20, 50 and 100 load increments. The curves of force versus relative vertical displacement (i.e., vertical displacement over initial height) for 10 and 100 l.i. are depicted in Fig. 11. The results are almost identical for all load discretizations (the relative error of the force at the end of the simulation computed with 10 l.i. is less than 0.6%). Fig. 12 shows the evolution of the distribution of the cone internal variable. As expected, the material response is clearly nonhomogeneous. Note that a wide region at the top of the sample does not enter in the softening regime ($\kappa_{\mathrm{con}} < 1$), even for large vertical displacements, while in the center of the sample (lower left corner of the computational domain) softening starts before the global limit force is reached.

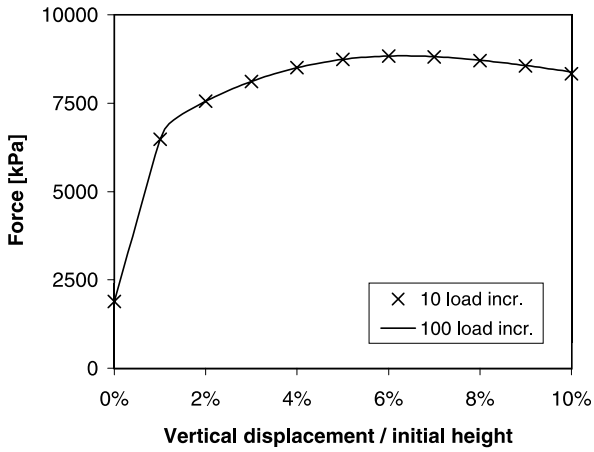

Fig. 11. Triaxial test problem. Force versus relative vertical displacement.

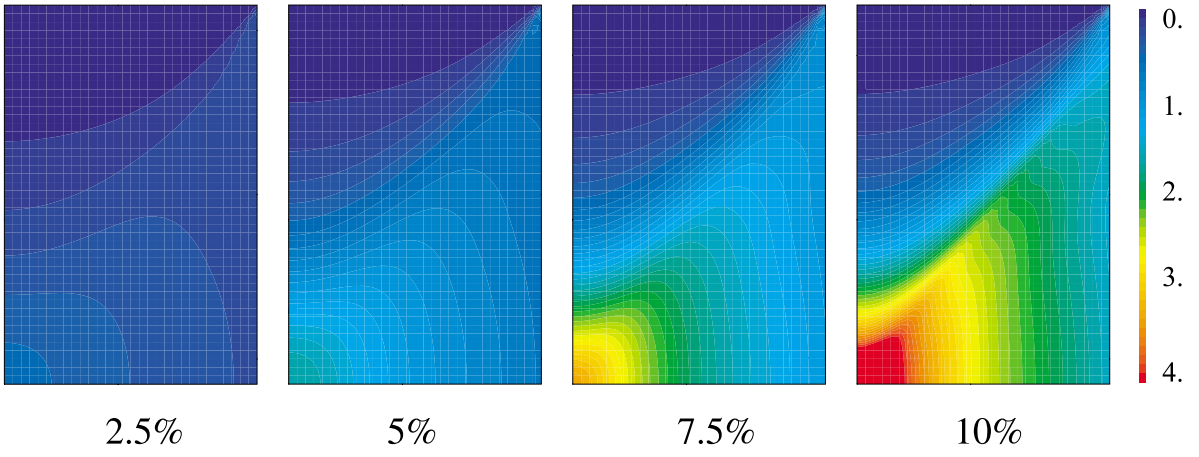

Fig. 12. Triaxial test problem. Distribution of the cone internal variable for different values of the relative vertical displacement.

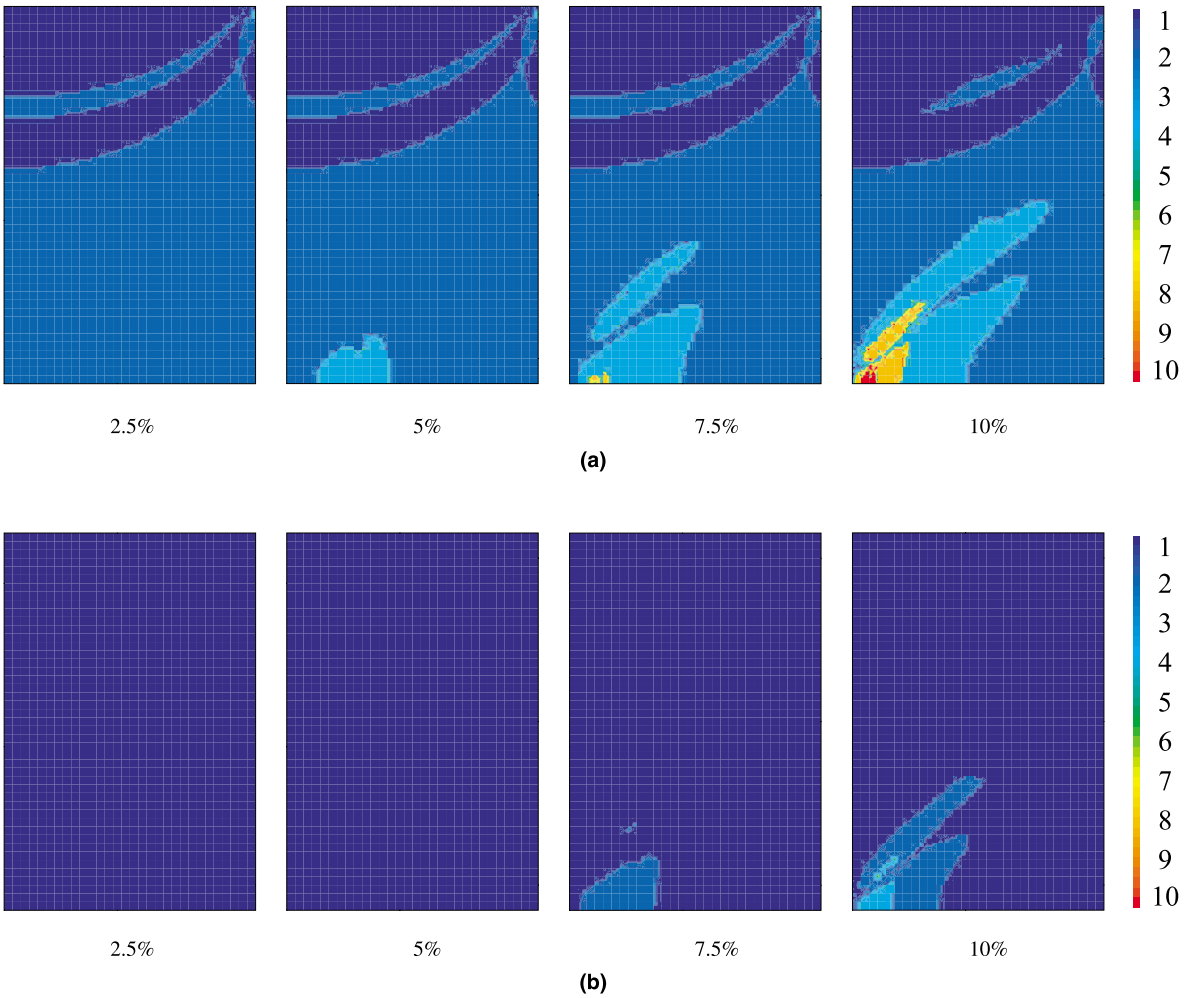

Fig. 13. Triaxial test problem. Distribution of the number of substeps required for different values of the relative vertical displacement. Problem solved with (a) 20 l.i., and (b) 50 l.i.

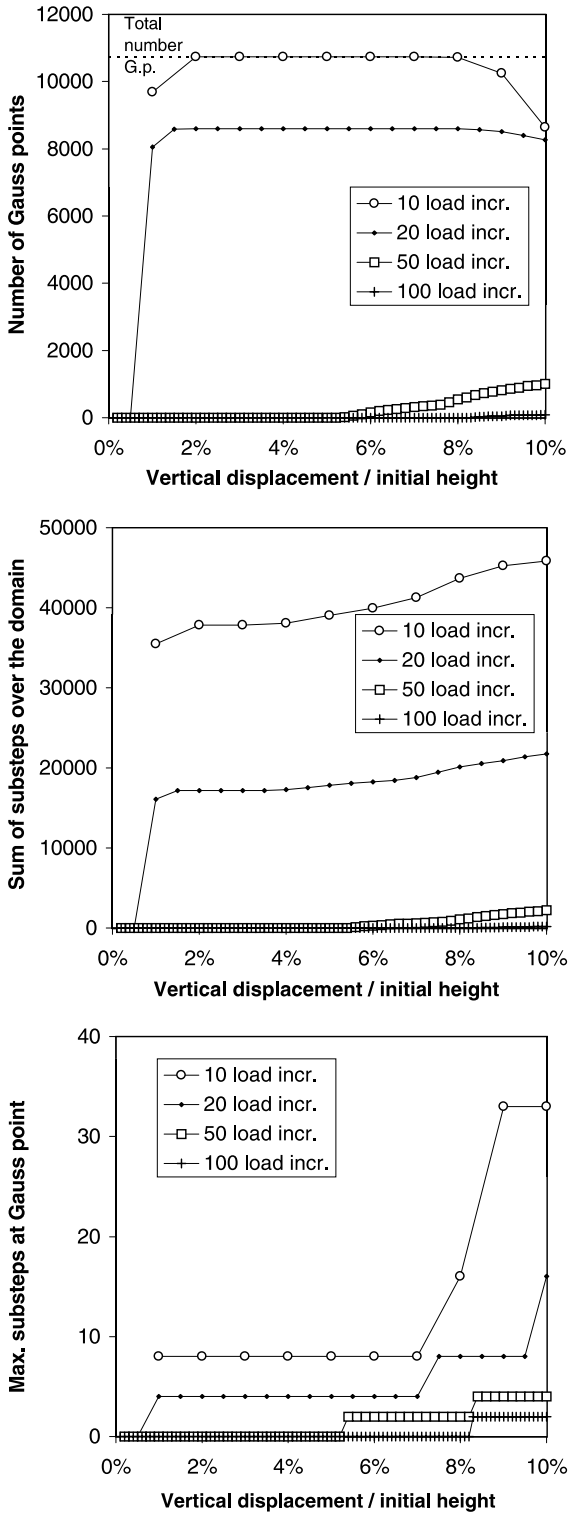

Fig. 14. Triaxial test problem. Evolution of the number of Gauss points with substepping activated (top), the sum of substeps over the domain (center) and the maximum number of substeps for all the Gauss points (bottom).

Fig. 13 shows the distribution of the number of substeps required at various load levels. Fig. 14 shows the evolution of the number of Gauss points with substepping activated, the sum of substeps over the domain and the maximum number of substeps for the four problems (with 10, 20, 50 and 100 l.i.). In the problems with 10 and 20 l.i., substepping is activated from the beginning of the analysis and almost everywhere in the domain. At the end of the test, part of the domain changes from plastic loading to elastic unloading. In that region, the substepping is deactivated. This results in a decrease in the number of Gauss points with substepping activated, see Figs. 13(a) and (14) (top). However, the number of substeps at each Gauss point is very low, compared with the previous example. On the other hand, with 50 l.i., substepping is activated only in the region of the domain where the local problems are more demanding. Finally, note that with 100 l.i. there are only a few Gauss points with substepping activated at the end of the test, and they require only two substeps.

The convergence results for several load levels and for the four problems (with 10, 20, 50 and 100 l.i.) are depicted in Fig. 15. Quadratic convergence is attained at all load levels and in the four problems. As in the previous example, the number of iterations per load increment decreases as the number of load increments increases. It is noticeable that the last load increments of the problem solved with 10 l.i., which correspond to a relative vertical displacement of 9% and 10%, require up to 13 and 18 iterations, respectively. Thus, although convergence is achieved, this load discretization is too coarse. On the other hand, the problem solved with 100 l.i. converges in four iterations at most during all the analysis.

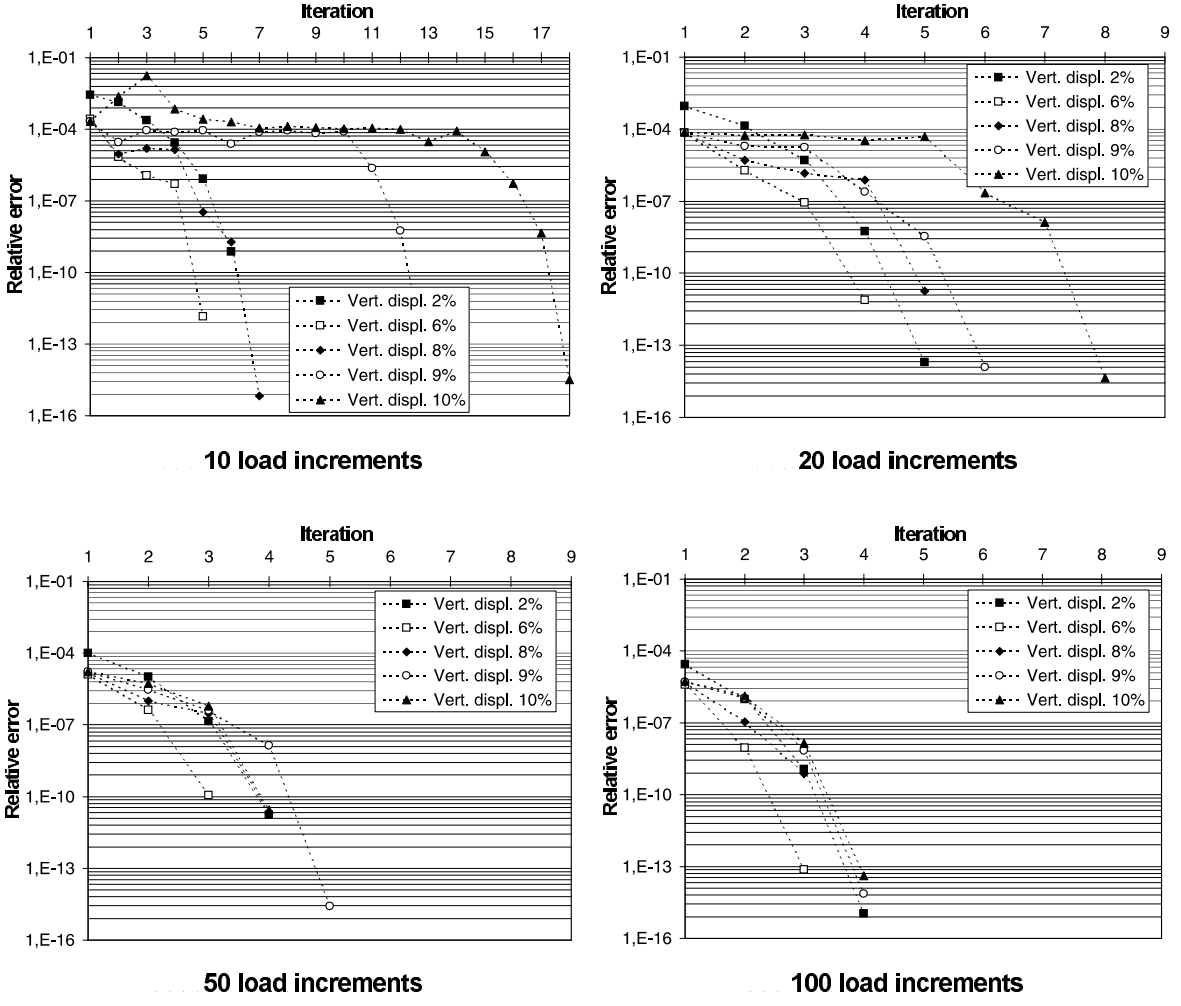

Fig. 15. Triaxial test problem. Convergence results for different values of the relative vertical displacement.

Table 2
Triaxial test problem. Relationship between number of global load increments and relative CPU time

Load increments	10	20	50	100
Relative CPU time	119%	100%	120%	215%

The computational cost (relative CPU time) of the four load discretizations is shown in Table 2. The solutions with 10, 20 and 50 l.i. have a similar computational cost. If only 10 or 20 l.i. are used, then substepping is activated in a large part of the domain, see Figs. (13)(a) and (14), and more global iterations per increment are needed. If 50 l.i. are used, then on the other hand, substepping is restricted to a smaller zone and less iterations per increment are required. This is why the total computational cost is similar in the three cases. It must be remarked, however, that the computational cost is halved with respect to the solution with 100 l.i., where almost no substepping is performed. In conclusion, the substepping scheme with consistent tangent matrix is computationally efficient.

5. Conclusions

A general expression of the consistent tangent matrix for substepping schemes has been presented. The consistent tangent moduli are computed via recursive linearization of the nonlinear constitutive equations within each substep. In each substep, any single-step scheme may be used. The expression for the generalized midpoint rule (which includes backward and forward Euler schemes as particular cases) has been derived. A simple and compact formula is obtained, with a structure very similar to the case with no substepping.

An adaptive substepping scheme based on the backward Euler rule has been chosen for illustrative purposes. Substepping is activated only at the Gauss points where the local problem requires more than a prescribed number of iterations. With this strategy, the most restrictive Gauss points no longer control the load increment of the global problem. This allows a large reduction of the number of load increments of the global problem, which typically implies a large reduction of the computational cost.

These aspects have been illustrated with the rounded hyperbolic Mohr–Coulomb model. The substepping scheme ensures local-level quadratic convergence over all the domain even for large load increments. The corresponding consistent tangent matrix presented in this paper ensures quadratic convergence at the global level. The combination of both techniques leads to a large reduction of computational cost.

Moreover, if needed, the derivatives required for the evaluation of the consistent tangent moduli can be approximated via numerical differentiation. With numerical differentiation, quadratic convergence is also attained, both at the local and the global levels. This has been illustrated with the MRS-Lade model.

From a practical viewpoint, it has been shown that the combination of consistent tangent matrices, substepping and numerical differentiation lead to the efficient and simple solving of complex nonlinear inelasticity problems.

Appendix A. Consistent tangent moduli for substepping with the generalized midpoint rule

In Section 3, each substep is integrated with the backward Euler rule. Here, the generalized midpoint rule [11], which includes the forward and backward Euler rules as particular cases, is considered. The expression of the consistent tangent moduli is obtained with the same ideas and notation of Section 3.

The nonlinear problem corresponding to a generic substep k integrated with the generalized midpoint integration rule is

$$\hat{\mathbf{f}}\left({}^{n+(k/m)}\boldsymbol{\sigma},\, {}^{n+(k/m)}\boldsymbol{\kappa},\, \lambda_k,\, {}^{n+((k-1)/m)}\boldsymbol{\sigma},\, {}^{n+((k-1)/m)}\boldsymbol{\kappa},\, \lambda_{k-1}\right) = \begin{pmatrix} \mathbf{I}_{n\sigma} & \mathbf{0}_{n\sigma,n\kappa} & \mathbf{0}_{n\sigma,1} \\ \mathbf{0}_{n\kappa,n\sigma} & \mathbf{I}_{n\kappa} & \mathbf{0}_{n\kappa,1} \\ \mathbf{0}_{1,n\sigma} & \mathbf{0}_{1,n\kappa} & 0 \end{pmatrix} \begin{pmatrix} {}^{n+((k-1)/m)}\boldsymbol{\sigma} \\ {}^{n+(k-1/m)}\boldsymbol{\kappa} \\ \lambda_{k-1} \end{pmatrix} + \begin{pmatrix} \mathbf{E} \\ \mathbf{0}_{n\kappa,1} \\ 0 \end{pmatrix} \Delta\boldsymbol{\epsilon}_k \tag{A.1}$$

with $\hat{\mathbf{f}}$ defined as

$$\hat{\mathbf{f}} = \begin{pmatrix} {}^{n+(k/m)}\boldsymbol{\sigma} + \lambda_k \mathbf{E}^{n+((k-1+\theta)/m)}\mathbf{m} \\ {}^{n+(k/m)}\boldsymbol{\kappa} - \lambda_k {}^{n+((k-1+\theta)/m)}\mathbf{h} \\ F\left({}^{n+(k/m)}\boldsymbol{\sigma}, {}^{n+(k/m)}\boldsymbol{\kappa}\right) \end{pmatrix} \tag{A.2}$$

and

$$\begin{aligned} {}^{n+(k-1+\theta/m)}\mathbf{m} &= \mathbf{m}\left({}^{n+((k-1+\theta)/m)}\boldsymbol{\sigma}, {}^{n+((k-1+\theta)/m)}\boldsymbol{\kappa}\right), \\ {}^{n+((k-1+\theta)/m)}\mathbf{h} &= \mathbf{h}\left({}^{n+((k-1+\theta)/m)}\boldsymbol{\sigma}, {}^{n+((k-1+\theta)/m)}\boldsymbol{\kappa}\right), \\ {}^{n+((k-1+\theta)/m)}\boldsymbol{\sigma} &= (1-\theta)^{n+((k-1)/m)}\boldsymbol{\sigma} + \theta^{n+(k/m)}\boldsymbol{\sigma}, \\ {}^{n+((k-1+\theta)/m)}\boldsymbol{\kappa} &= (1-\theta)^{n+((k-1)/m)}\boldsymbol{\kappa} + \theta^{n+(k/m)}\boldsymbol{\kappa}. \end{aligned} \tag{A.3}$$

In Eqs. (A.2) and (A.3), θ can range from $\theta = 0$ (forward Euler rule) to $\theta = 1$ (backward Euler rule). The variable λ_{k-1} has been included in both sides of Eq. (A.1) in order to simplify the following deduction of the consistent tangent moduli.

Note that for $\theta = 1$ the backward Euler scheme is recovered, and Eqs. (A.1) and (A.2) coincide with Eqs. (8) and (9), respectively.

Both sides of Eq. (A.1) are linearized with respect to $\Delta\boldsymbol{\epsilon}$,

$$\begin{aligned} &\frac{\partial \hat{\mathbf{f}}}{\partial\left({}^{n+(k/m)}\boldsymbol{\sigma}, {}^{n+(k/m)}\boldsymbol{\kappa}, \lambda_k\right)} \frac{\mathrm{d}\left({}^{n+(k/m)}\boldsymbol{\sigma}, {}^{n+(k/m)}\boldsymbol{\kappa}, \lambda_k\right)}{\mathrm{d}\Delta\boldsymbol{\epsilon}} + \frac{\partial \hat{\mathbf{f}}}{\partial\left({}^{n+((k-1)/m)}\boldsymbol{\sigma}, {}^{n+((k-1)/m)}\boldsymbol{\kappa}, \lambda_{k-1}\right)} \\ &\quad \times \frac{\mathrm{d}\left({}^{n+((k-1)/m)}\boldsymbol{\sigma}, {}^{n+((k-1)/m)}\boldsymbol{\kappa}, \lambda_{k-1}\right)}{\mathrm{d}\Delta\boldsymbol{\epsilon}} \\ &\quad = \begin{pmatrix} \mathbf{I}_{n\sigma+n\kappa} & \mathbf{0}_{n\sigma+n\kappa,1} \\ \mathbf{0}_{1,n\sigma+n\kappa} & 0 \end{pmatrix} \frac{\mathrm{d}\left({}^{n+((k-1)/m)}\boldsymbol{\sigma}, {}^{n+((k-1)/m)}\boldsymbol{\kappa}, \lambda_{k-1}\right)}{\mathrm{d}\Delta\boldsymbol{\epsilon}} + \alpha_k \begin{pmatrix} \mathbf{E} \\ \mathbf{0}_{n\kappa,n\sigma} \\ \mathbf{0}_{1,n\sigma} \end{pmatrix}. \end{aligned} \tag{A.4}$$

The derivatives of $\hat{\mathbf{f}}$ can be expressed as

$$\begin{aligned} \frac{\partial \hat{\mathbf{f}}}{\partial\left({}^{n+(k/m)}\boldsymbol{\sigma}, {}^{n+(k/m)}\boldsymbol{\kappa}, \lambda_k\right)} &= {}^{n+(k/m)}\mathbf{J}_\theta \\ &= \begin{pmatrix} \theta\lambda_k \mathbf{E}\frac{\partial \mathbf{m}}{\partial \boldsymbol{\sigma}} & \theta\lambda_k \mathbf{E}\frac{\partial \mathbf{m}}{\partial \boldsymbol{\kappa}} & \mathbf{E}\mathbf{m} \\ -\theta\lambda_k \frac{\partial \mathbf{h}}{\partial \boldsymbol{\sigma}} & -\theta\lambda_k \frac{\partial \mathbf{h}}{\partial \boldsymbol{\kappa}} & -\mathbf{h} \\ \mathbf{0}_{1,n\sigma} & \mathbf{0}_{1,n\kappa} & 0 \end{pmatrix}_{t={}^{n+((k-1+\theta)/m)}t} + \begin{pmatrix} \mathbf{I}_{n\sigma} & \mathbf{0}_{n\sigma,n\kappa} & \mathbf{0}_{n\sigma,1} \\ \mathbf{0}_{n\kappa,n\sigma} & \mathbf{I}_{n\kappa} & \mathbf{0}_{n\kappa,1} \\ \mathbf{n}^{\mathrm{T}} & \boldsymbol{\xi}^{\mathrm{T}} & 0 \end{pmatrix}_{t={}^{n+(k/m)}t} \end{aligned} \tag{A.5}$$

and

$$\frac{\partial \hat{\mathbf{f}}}{\partial\left({}^{n+((k-1)/m)}\boldsymbol{\sigma}, {}^{n+((k-1)/m)}\boldsymbol{\kappa}, \lambda_{k-1}\right)} = \begin{pmatrix} (1-\theta)\lambda_k \mathbf{E}\frac{\partial \mathbf{m}}{\partial \boldsymbol{\sigma}} & (1-\theta)\lambda_k \mathbf{E}\frac{\partial \mathbf{m}}{\partial \boldsymbol{\kappa}} & \mathbf{0}_{n\sigma,1} \\ -(1-\theta)\lambda_k \frac{\partial \mathbf{h}}{\partial \boldsymbol{\sigma}} & -(1-\theta)\lambda_k \frac{\partial \mathbf{h}}{\partial \boldsymbol{\kappa}} & \mathbf{0}_{n\kappa,1} \\ \mathbf{0}_{1,n\sigma} & \mathbf{0}_{1,n\kappa} & 0 \end{pmatrix}_{t={}^{n+((k-1+\theta)/m)}t}. \tag{A.6}$$

Assuming that $\det({}^{n+(k/m)}\mathbf{J}_\theta) \neq 0$ and after some arrangements, Eq. (A.4) is rewritten as

$$\frac{\mathrm{d}\left({}^{n+(k/m)}\boldsymbol{\sigma}, {}^{n+(k/m)}\boldsymbol{\kappa}, \lambda_k\right)}{\mathrm{d}\Delta\boldsymbol{\epsilon}} = \left({}^{n+(k/m)}\mathbf{J}_\theta\right)^{-1} \left(\alpha_k \mathbf{P}\mathbf{E} + {}^{n+(k/m)}\mathbf{G}_\theta \frac{\mathrm{d}\left({}^{n+((k-1)/m)}\boldsymbol{\sigma}, {}^{n+((k-1)/m)}\boldsymbol{\kappa}, \lambda_{k-1}\right)}{\mathrm{d}\Delta\boldsymbol{\epsilon}}\right) \tag{A.7}$$

with

$${}^{n+(k/m)}\mathbf{G}_\theta = \begin{pmatrix} \left(\mathbf{I}_{n\sigma} - (1-\theta)\lambda_k \mathbf{E}\frac{\partial \mathbf{m}}{\partial \boldsymbol{\sigma}}\right) & -(1-\theta)\lambda_k \mathbf{E}\frac{\partial \mathbf{m}}{\partial \boldsymbol{\kappa}} & \mathbf{0}_{n\sigma,1} \\ (1-\theta)\lambda_k \frac{\partial \mathbf{h}}{\partial \boldsymbol{\sigma}} & \left(\mathbf{I}_{n\kappa} + (1-\theta)\lambda_k \frac{\partial \mathbf{h}}{\partial \boldsymbol{\kappa}}\right) & \mathbf{0}_{n\kappa,1} \\ \mathbf{0}_{1,n\sigma} & \mathbf{0}_{1,n\kappa} & 0 \end{pmatrix}_{t={}^{n+((k-1+\theta)/m)}t}. \tag{A.8}$$

The first substep is linearized into

$$\frac{\mathrm{d}\left({}^{n+(1/m)}\boldsymbol{\sigma},\,{}^{n+(1/m)}\boldsymbol{\kappa},\,\lambda_1\right)}{\mathrm{d}\Delta\boldsymbol{\epsilon}} = \alpha_1\left({}^{n+(1/m)}\mathbf{J}_\theta\right)^{-1}\mathbf{PE}. \tag{A.9}$$

Finally, following the same process of Section 3, the consistent tangent moduli are obtained. The final expression is

$$\frac{\mathrm{d}^{n+1}\boldsymbol{\sigma}}{\mathrm{d}\Delta\boldsymbol{\epsilon}} = \mathbf{P}^{\mathrm{T}}\left[\sum_{i=1}^{m}\left(\alpha_i\prod_{j=m}^{i}{}^{n+(j/m)}\mathbf{A}_\theta\right)\right]\mathbf{PE}, \tag{A.10}$$

where $\forall k \in \{1,\ldots,m-1\}$,

$${}^{n+(k/m)}\mathbf{A}_\theta = {}^{n+((k+1)/m)}\mathbf{G}_\theta\left({}^{n+(k/m)}\mathbf{J}_\theta\right)^{-1} \tag{A.11}$$

and for $k = m$,

$${}^{n+1}\mathbf{A}_\theta = \left({}^{n+1}\mathbf{J}_\theta\right)^{-1}. \tag{A.12}$$

For the particular case of $\theta = 1$ (backward Euler scheme) Eq. (A.10) reduces to Eq. (18).

A.1. Consistent tangent moduli for substepping with the forward Euler method

In general, numerical inversion of the Jacobian matrices is required to compute the consistent tangent moduli, see Eqs. (A.11) and (A.12). However, for the particular case of $\theta = 0$ (forward Euler method), a closed-form expression of the inverse of the Jacobian can be derived, so numerical inversion is not needed.

The Jacobian is

$${}^{n+(k/m)}\mathbf{J}_0 = \begin{pmatrix} \mathbf{I}_{n\sigma} & \mathbf{0}_{n\sigma,n\kappa} & \mathbf{E}^{n+((k-1)/m)}\mathbf{m} \\ \mathbf{0}_{n\kappa,n\sigma} & \mathbf{I}_{n\kappa} & -{}^{n+((k-1)/m)}\mathbf{h} \\ {}^{n+(k/m)}\mathbf{n}^{\mathrm{T}} & {}^{n+(k/m)}\boldsymbol{\xi}^{\mathrm{T}} & 0 \end{pmatrix}, \tag{A.13}$$

and its inverse is

$$\left({}^{n+(k/m)}\mathbf{J}_0\right)^{-1} = \begin{pmatrix} \left(\mathbf{I}_{n\sigma} - a\mathbf{E}\mathbf{m}\mathbf{n}^{\mathrm{T}}\right) & -a\mathbf{E}\mathbf{m}\boldsymbol{\xi}^{\mathrm{T}} & a\mathbf{E}\mathbf{m} \\ a\mathbf{h}\mathbf{n}^{\mathrm{T}} & \left(\mathbf{I}_{n\kappa} + a\mathbf{h}\boldsymbol{\xi}^{\mathrm{T}}\right) & -a\mathbf{h} \\ a\mathbf{n}^{\mathrm{T}} & a\boldsymbol{\xi}^{\mathrm{T}} & -a \end{pmatrix}, \tag{A.14}$$

where $\mathbf{n}$ and $\boldsymbol{\xi}$ are referred to time ${}^{n+(k/m)}t$, $\mathbf{m}$ and $\mathbf{h}$ to ${}^{n+((k-1)/m)}t$, and with

$$a = \frac{1}{\mathbf{n}^{\mathrm{T}}\mathbf{E}\mathbf{m} - \boldsymbol{\xi}^{\mathrm{T}}\mathbf{h}}. \tag{A.15}$$

Eqs. (A.14) and (A.15) can be obtained using Sherman and Morrison's lemma [20]. Note that these equations only involve matrix products.

Appendix B. Computationally efficient expression of the consistent tangent moduli for substepping with the backward Euler method

The expression of the consistent tangent moduli obtained in Section 3, Eq. (18), can be rearranged to render it computationally more efficient. In the following, an equivalent expression that involves smaller matrices is presented. In the new expression, moreover, the computation of the inverse of the Jacobians is simplified.

First, the equivalence

$$\begin{pmatrix} \mathbf{I}_{n\sigma} & \mathbf{0}_{n\sigma,n\kappa} & \mathbf{0}_{n\sigma,1} \\ \mathbf{0}_{n\kappa,n\sigma} & \mathbf{I}_{n\kappa} & \mathbf{0}_{n\kappa,1} \\ \mathbf{0}_{1,n\sigma} & \mathbf{0}_{1,n\kappa} & 0 \end{pmatrix} = \begin{pmatrix} \mathbf{I}_{n\sigma} & \mathbf{0}_{n\sigma,n\kappa} \\ \mathbf{0}_{n\kappa,n\sigma} & \mathbf{I}_{n\kappa} \\ \mathbf{0}_{1,n\sigma} & \mathbf{0}_{1,n\kappa} \end{pmatrix} \begin{pmatrix} \mathbf{I}_{n\sigma} & \mathbf{0}_{n\sigma,n\kappa} & \mathbf{0}_{n\sigma,1} \\ \mathbf{0}_{n\kappa,n\sigma} & \mathbf{I}_{n\kappa} & \mathbf{0}_{n\kappa,1} \end{pmatrix} \tag{B.1}$$

is employed in order to rewrite Eq. (13) into

$$\frac{\mathrm{d}\left({}^{n+(k/m)}\boldsymbol{\sigma}, {}^{n+(k/m)}\boldsymbol{\kappa}, \lambda_k\right)}{\mathrm{d}\Delta\boldsymbol{\epsilon}} = \left({}^{n+(k/m)}\mathbf{J}\right)^{-1} \begin{pmatrix} \mathbf{I}_{n\sigma} & \mathbf{0}_{n\sigma,n\kappa} \\ \mathbf{0}_{n\kappa,n\sigma} & \mathbf{I}_{n\kappa} \\ \mathbf{0}_{1,n\sigma} & \mathbf{0}_{1,n\kappa} \end{pmatrix} \left(\begin{pmatrix} \mathbf{I}_{n\sigma} & \mathbf{0}_{n\sigma,n\kappa} & \mathbf{0}_{n\sigma,1} \\ \mathbf{0}_{n\kappa,n\sigma} & \mathbf{I}_{n\kappa} & \mathbf{0}_{n\kappa,1} \end{pmatrix} \frac{\mathrm{d}\left({}^{n+((k-1)/m)}\boldsymbol{\sigma}, {}^{n+((k-1)/m)}\boldsymbol{\kappa}, \lambda_{k-1}\right)}{\mathrm{d}\Delta\boldsymbol{\epsilon}} + \alpha_k \begin{pmatrix} \mathbf{E} \\ \mathbf{0}_{n\kappa,n\sigma} \end{pmatrix} \right). \tag{B.2}$$

Then, Eq. (B.2) is premultiplied by

$$\begin{pmatrix} \mathbf{I}_{n\sigma} & \mathbf{0}_{n\sigma,n\kappa} & \mathbf{0}_{n\sigma,1} \\ \mathbf{0}_{n\kappa,n\sigma} & \mathbf{I}_{n\kappa} & \mathbf{0}_{n\kappa,1} \end{pmatrix} \tag{B.3}$$

in order to get

$$\frac{\mathrm{d}\left({}^{n+(k/m)}\boldsymbol{\sigma}, {}^{n+(k/m)}\boldsymbol{\kappa}\right)}{\mathrm{d}\Delta\boldsymbol{\epsilon}} = {}^{n+(k/m)}\mathbf{A}_{\mathrm{c}} \left(\frac{\mathrm{d}\left({}^{n+((k-1)/m)}\boldsymbol{\sigma}, {}^{n+((k-1)/m)}\boldsymbol{\kappa}\right)}{\mathrm{d}\Delta\boldsymbol{\epsilon}} + \alpha_k \mathbf{P}_{\mathrm{c}}\mathbf{E} \right), \tag{B.4}$$

where

$$\mathbf{P}_{\mathrm{c}} = \begin{pmatrix} \mathbf{I}_{n\sigma} \\ \mathbf{0}_{n\kappa,n\sigma} \end{pmatrix}, \quad {}^{n+(k/m)}\mathbf{A}_{\mathrm{c}} = \begin{pmatrix} \mathbf{I}_{n\sigma} & \mathbf{0}_{n\sigma,n\kappa} & \mathbf{0}_{n\sigma,1} \\ \mathbf{0}_{n\kappa,n\sigma} & \mathbf{I}_{n\kappa} & \mathbf{0}_{n\kappa,1} \end{pmatrix} \left({}^{n+(k/m)}\mathbf{J}\right)^{-1} \begin{pmatrix} \mathbf{I}_{n\sigma} & \mathbf{0}_{n\sigma,n\kappa} \\ \mathbf{0}_{n\kappa,n\sigma} & \mathbf{I}_{n\kappa} \\ \mathbf{0}_{1,n\sigma} & \mathbf{0}_{1,n\kappa} \end{pmatrix}, \tag{B.5}$$

and use is made of the relation

$$\begin{pmatrix} \mathbf{I}_{n\sigma} & \mathbf{0}_{n\sigma,n\kappa} & \mathbf{0}_{n\sigma,1} \\ \mathbf{0}_{n\kappa,n\sigma} & \mathbf{I}_{n\kappa} & \mathbf{0}_{n\kappa,1} \end{pmatrix} \frac{\mathrm{d}\left({}^{n+(k/m)}\boldsymbol{\sigma}, {}^{n+(k/m)}\boldsymbol{\kappa}, \lambda_k\right)}{\mathrm{d}\Delta\boldsymbol{\epsilon}} = \frac{\mathrm{d}\left({}^{n+(k/m)}\boldsymbol{\sigma}, {}^{n+(k/m)}\boldsymbol{\kappa}\right)}{\mathrm{d}\Delta\boldsymbol{\epsilon}}. \tag{B.6}$$

Finally, following the same process of Section 3, the consistent tangent moduli are obtained. The final expression is

$$\frac{\mathrm{d}^{n+1}\boldsymbol{\sigma}}{\mathrm{d}\Delta\boldsymbol{\epsilon}} = \mathbf{P}_{\mathrm{c}}^{\mathrm{T}} \left[\sum_{i=1}^{m} \left(\alpha_i \prod_{j=m}^{i} {}^{n+(j/m)}\mathbf{A}_{\mathrm{c}} \right) \right] \mathbf{P}_{\mathrm{c}}\mathbf{E}. \tag{B.7}$$

Eq. (B.7) has the same structure of Eq. (18). However, the matrices involved here are smaller. In fact, the consistent tangent moduli are computed with the following expression:

$$\frac{\mathrm{d}^{n+1}\boldsymbol{\sigma}}{\mathrm{d}\Delta\boldsymbol{\epsilon}} = \mathbf{P}_{\mathrm{c}}^{T\,n+1}\mathbf{A}_{\mathrm{c}}(\alpha_m\mathbf{P}_{\mathrm{c}} + {}^{n+((m-1)/m)}\mathbf{A}_{\mathrm{c}}(\alpha_{m-1}\mathbf{P}_{\mathrm{c}} + \cdots(\alpha_2\mathbf{P}_{\mathrm{c}} + \alpha_1{}^{n+(1/m)}\mathbf{A}_{\mathrm{c}}\mathbf{P}_{\mathrm{c}}\underbrace{)\cdots)}_{m-1})\mathbf{E}, \tag{B.8}$$

which is equivalent to Eq. (B.7). As suggested by Eq. (B.8), the consistent tangent moduli are computed recursively during time-integration: when the substep j is integrated, the matrix ${}^{n+(j/m)}\mathbf{A}_{\mathrm{c}}$ is computed and the corresponding part of the consistent tangent moduli is calculated. The process is always the same, except for the first and the last substeps.

Moreover, because of the special structure of the Jacobian, the matrices ${}^{n+(j/m)}\mathbf{A}_{\mathrm{c}}$ are computed inverting only the leading principal minor of order $n\sigma + n\kappa$ of the Jacobian. This result can be obtained using Sherman and Morrison's lemma [20].

References

[1] J.C. Simo, R.L. Taylor, Consistent tangent operators for rate-independent elastoplasticity, Comput. Methods Appl. Mech. Engrg. 48 (1985) 101–118.

[2] N. Bićanić, C.J. Pearce, Computational aspects of a softening plasticity model for plain concrete, Mech. Cohesive Frictional Mater. 1 (1996) 75–94.

[3] A. Pérez-Foguet, F. Armero. On the formulation of closest-point projection algorithms in elastoplasticity. Part II: globally convergent schemes, Int. J. Numer. Methods Engrg. 2000, Submitted for publication.

[4] S.W. Sloan, Substepping schemes for the numerical integration of elastoplastic stress –strain relations, Int. J. Numer. Methods Engrg. 24 (1987) 893–911.

[5] A.J. Abbo, S.W. Sloan, An automatic load stepping algorithm with error control, Int. J. Numer. Methods Engrg. 39 (1996) 1737–1759.

[6] A.J. Abbo, S.W. Sloan, A smooth hyperbolic approximation to the Mohr–Coulomb yield criterion, Comput. Struct. 54 (3) (1995) 427–441.

[7] A. Pérez-Foguet, A. Rodríguez-Ferran, A. Huerta, Numerical differentiation for local and global tangent operators in computational plasticity, Comput. Methods Appl. Mech. Engrg. 189 (2000) 277–296.

[8] A. Pérez-Foguet, A. Rodríguez-Ferran, A. Huerta, Numerical differentiation for non-trivial consistent tangent matrices: an application to the MRS-Lade model, Int. J. Numer. Methods Engrg. 48 (2000) 159–184.

[9] S. Sture, K. Runesson, E.J. Macari-Pasqualino, Analysis and calibration of a three-invariant plasticity model for granular materials, Ingenieur Arquiv 59 (1989) 253–266.

[10] A. Pérez-Foguet, A. Huerta, Plastic flow potential for the cone region of the MRS-Lade model, J. Engrg. Mech. 125 (3) (1999) 364–367.

[11] M. Ortiz, E.P. Popov, Accuracy and stability of integration algorithms for elastoplastic constitutive relations, Int. J. Numer. Methods Engrg. 21 (1985) 1561–1576.

[12] J.C. Simo, T.J.R. Hughes, Computational Inelasticity, Springer (1998).

[13] M.A. Crisfield, Non-linear Finite Element Analysis of Solids and Structures. 1 Essentials, Wiley, Chichester, 1991.

[14] K. Runesson, A. Samuelsson, L. Bernspang, Numerical technique in plasticity including solution advancement control, Int. J. Numer. Methods Engrg. 22 (1986) 769–788.

[15] M. Ortiz, J.B. Martin, Symmetry-preserving return mapping algorithms and incrementally extremal paths a unification of concepts, Int. J. Numer. Methods Engrg. 28 (1989) 1839–1853.

[16] E.J. Macari, K. Runesson, S. Sture, Response prediction of granular materials at low effective stresses, J. Geotech. Engrg. 120 (1994) 1252–1268.

[17] E.J. Macari, S. Weihe, P. Arduino, Implicit integration of elastoplastic constitutive models for frictional materials with highly non-linear hardening functions, Mech. Cohesive Frictional Mater. 2 (1994) 1–29.

[18] B. Jeremić, S. Sture, Implicit integrations rules in plasticity: Theory and implementation, Technical Report, Report to NASA Marshall Space Flight Center, Contract: NAS8-38779, University of Colorado at Boulder, July 1994.

[19] J.W. Rudnicki, J.R. Rice, Conditions of the localization of deformation in pressure-sensitive dilatant materials, J. Mech. Phys. Solids 23 (1975) 371–394.

[20] J.E. Dennis, J.J. Moré, Quasi-Newton methods motivations and theory, SIAM Rev. 19 (1977) 46–89.